PERGAMON

International Journal of Solids and Structures 40 (2003) 1973–1993

INTERNATIONAL JOURNAL OF SOLIDS and STRUCTURES

www.elsevier.com/locate/ijsolstr

A coupled IEM/FEM approach for solving elastic problems with multiple cracks

D.S. Liu *, D.Y. Chiou

Department of Mechanical Engineering, National Chung Cheng University, 160, San-Hsing, Ming-Hsiung, Chia-Yi, 621, Taiwan, R.O.C.

Received 12 March 2002; received in revised form 11 December 2002

Abstract

In this paper, the detailed two-dimensional infinite element method (IEM) formulation with infinite element (IE)–finite element (FE) coupling scheme for investigating mode I stress intensity factor in elastic problems with imbedded geometric singularities (e.g. cracks) is presented. The IE–FE coupling algorithm is also successfully extended to solve multiple crack problems. In this method, the domain of the primary problem is subdivided into two sub-domains modeled separately using the IEM for the multiple crack sub-domain, and the FEM for the uncracked sub-domain. In the IE sub-domain, the similarity partition concept together with the IEM formulation are employed to automatically generate a large number of infinitesimal elements, layer by layer, around the tip of each crack. All degrees of freedom related to the IE sub-domain, except for those associated with the coupling interface, are condensed and transformed to form a finite master IE for each crack with master nodes on sub-domain boundary only. All of the stiffness matrices constructed in the IE sub-domains are assembled into the system stiffness matrix for the FE sub-domain. The resultant FE solution with a symmetrical stiffness matrix, having the singularity effect of imbedded cracks in IEs, is required only for solving multiple crack problems.

Using these efficient numerical techniques a very fine mesh pattern can be established around each crack tip without increasing the degree of freedom of the global FEM solution. One is easily allowed to conduct parametric analyses for various crack sizes without changing the FE mesh. Numerical examples are presented to show the performance of the proposed method and compared with the corresponding known results where available.

Keywords: Infinite element method; Finite element method; Multiple crack problem; Stress intensity factor

1. Introduction

The stress analysis of an elastic body with imbedded geometric singularities (e.g. cracks, dissimilar material junctions, re-entrant corners, etc.) is a topic of practical importance in a broad variety of engineering applications. The finite element method (FEM) is the most popular and well-developed method for analyzing such problems (Chan et al., 1970; Buettner and Quesnel, 1993; Su et al., 2001). However, it is well

* Corresponding author. Tel.: +886-5-2720411x33305; fax: +886-5-2720589.
E-mail address: imedsl@ccunix.ccu.edu.tw (D.S. Liu).

0020-7683/02/$ - see front matter © 2002 Elsevier Science Ltd. All rights reserved.
doi:10.1016/S0020-7683(03)00014-3

known that direct application of the FEM to model the singularity point vicinity requires local refinement, which in turn requires a great number of elements, extensive computer memory, and converges very slowly because of deficiencies in the singularity representation. To overcome these difficulties, special elements such as singular elements (Yosibash and Szabó, 1995; Tan and Meguid, 1996), hybrid elements (Kang and De Saxcé, 1992; Chow et al., 1995; Leung and Su, 1995), and global–local elements (Mote, 1971; Her, 2000; Barut et al., 2001) were developed to model the crack region combined with a system stiffness matrix. Only a few degrees of freedom are required to model the singular behavior ahead of the crack tip. However, some of these applications are limited to solving single crack problems with simplified load conditions. Besides, some of the special element shapes are fixed to certain shape types (e.g. a round or rectangular shapes) that also prevent them from being easily combined with the existing FEM codes. Another attractive and powerful computational technique is to model the singularity region using the boundary element method (BEM). The BEM is based on an integral equation formulation and requires discretization of the problem boundary only. A wide variety of elastic crack problems have been successfully analyzed using BEM (Cruse, 1988; Xiao and Hui, 1994; Kermanidis and Mavrothanasis, 1995; Sladek and Sladek, 1995; Katsareas and Anifantis, 1995; Yan and Nguyen-Dang, 1995; Bois-Grossiant and Tan, 1995; Ang and Clements, 1995; Hasebe et al., 1996; Mukhopadhyay et al., 1998). The detailed descriptions are not mentioned here. The subsequent developments in BEM, such as the variable singularity boundary element (Mukhopadhyay et al., 2000), combined BEM with evolutionary algorithms (Burczynski and Beluch, 2001) and hypersingular BEM accelerated with fast multipole method (Yoshida et al., 2001) were recently proposed for improving the solution accuracy and providing fast computational speed in computation. In spite of the many BEM advantages, it still has several drawbacks. To derive the BEM integral equation formulation, a fundamental singular solution is needed that satisfies the governing differential equation in the domain as basis functions for an approximate solution that has difficulty in considering inhomogeneous behavior. Moreover, the global solution matrices formed from BEM are generally fully populated and non-symmetrical, leading to solve the solutions by time consuming direct inverse methods that are difficult to link with FEM for large sized industrial applications.

Mathematicians devised an alternate numerical method called the "infinite element method" (IEM) in the 1970s to deal with geometric singular problems. The basic idea behind IEM is to discretize the problem domain using a group of countable infinity elements with a designed nodal sequence so that each element-layer is similar to the other layers (unvaried stiffness). This concept was proposed first by Silvester and Cermark (1969) using the finite difference method. Recently, Go and Lin (1991) and Go and Chen (1992) applied this concept with a mesh generation scheme to solve stress singularity problems. Their works were limited to dealing with finite layers with similar elements and could not assure that the numerical solutions would converge. Thatcher (1975, 1978) used infinite numbers of elements and derived a recurrence relation for the Laplace' equation in a systematic way to solve problems with re-entrant corners and unbounded domains. At the same time, Ying (1978, 1992), Han and Ying (1979), and Ying and Pan (1981) independently developed the mathematical foundations of an IEM formulation for the Laplace' equation, plane elasticity problems, corner problem and exterior stokes problems. Ying (1992) proved that there exists a transformation matrix to relate the nodal displacement vector between the inner and outer layers, therefore the total stiffness matrix could degenerate to form a combined stiffness matrix related only to boundary nodes and tractions. More importantly, he proved that the combined stiffness matrix is a semi-positive definite matrix that could converge to a certain constant quantity when the number of layers approached to infinity. Several simple examples were presented to demonstrate the IEM accuracy without describing the detailed numerical procedure. Guo (1979) proved that the concept of similar elements could be extended to arbitrary isoparametric elements. He also constructed a transformation procedure to combine the local stiffness matrix layer to layer. No numerical examples were presented in his paper. As a consequence, FEM can solve problems with complicated domain and boundary conditions but cannot manage for singularity areas in the domain. Conversely, IEM is suitable for solving singularity problems but is applicable only for

relatively simpler shaped domains. A better strategy involves combining both methods to deal with all kinds of singularity problems.

In this paper, the algorithms derived in previous studies (Guo, 1979; Ying, 1992) are worked out in detail to construct an IEM numerical procedure, which is extended in combination with FEM to solve multi-crack problems. In this method each crack tip occupies a sub-domain with an arbitrary but relatively simple shape (e.g. rectangular shape) surrounding the crack tip. The similarity partition concept and IEM formulation are employed to automatically generate a large number of infinitesimal elements layer by layer distributed over the IE sub-domain. All degrees of freedom related to each IE sub-domain, except for those associated with the coupling interface, are condensed and transformed to form an equivalent combined element with master nodes degrees of freedom only. This is regarded as a regular finite element and called "infinite element" (IE). All other crack tips with similar IE sub-domains will have the same IE stiffness matrix. Finally, all the stiffness matrices constructed in the IE sub-domains are assembled into the system stiffness matrix for the FE sub-domain. The resultant FE solution with a symmetrical stiffness matrix, having the singularity effect of imbedded cracks in IEs, is required only for solving multiple crack problems. Because the IEM solutions are given only in the vicinity of the crack tips, the solutions outside the singular regions are obtained using the conventional FEM. The advantage of being able to model complex boundary conditions and maintain the mesh refinement effect is therefore preserved.

A convergence criterion is proposed for the IEM formulation to extend the imaginary "infinity layer" concept into practical actualization, and assure that the numerical solutions of the IE stiffness matrix will converge. No prior governing assumption is required and no special FEs, such as singular, hybrid and boundary elements, need be incorporated. No further parametric refinement analysis is needed because of the high IEM formulation convergence. Numerical examples are presented and compared with the corresponding known results to validate the accuracy of the IEM and IEM/FEM codes and show the performance of the proposed method.

2. Infinite element modeling formulation

2.1. Similarity of two-dimensional isoparametric elements

As mentioned earlier, the similar partition concept is the key to the IEM. This concept can be illustrated using the two similar general quadrilateral elements shown in Fig. 1. For element I, the local nodes i are numbered 1, 2, 3, and 4 in the counterclockwise direction. $(x_i^{\mathrm{I}}, y_i^{\mathrm{I}})$ denotes the global coordinate value of node i. Taking the global origin O and ξ as the center of the similarity and proportionality ratio, one creates element II, whose nodal coordinate value and length dimensions are similar to those of element I. The relationship between the corresponding nodes can be expressed as

$$(x_i^{\mathrm{II}}, y_i^{\mathrm{II}}) = (\xi x_i^{\mathrm{I}}, \xi y_i^{\mathrm{I}}) \tag{1}$$

where $\xi \in (0,1)$ or $\xi \in (1,\infty)$, which implies the scale ratio. From the isoparametric representation, shape functions are used to express the coordinates of a point within element I in terms of the nodal coordinates. Thus we have

$$x^{\mathrm{I}} = \sum_{i=1}^{4} \phi_i(\zeta,\eta) x_i^{\mathrm{I}} \tag{2}$$

$$y^{\mathrm{I}} = \sum_{i=1}^{4} \phi_i(\zeta,\eta) y_i^{\mathrm{I}} \tag{3}$$

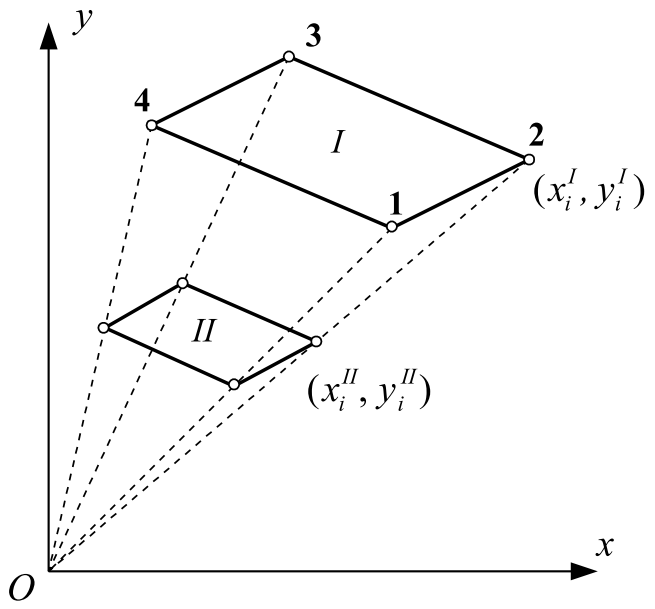

Fig. 1. Schematic diagram for similar 2-D elements (source: Guo, 1979).

Multiplying both sides by ξ and in view of Eq. (1)

$$x^{\mathrm{II}} = \xi x^{\mathrm{I}} = \sum_{i=1}^{4} \phi_i(\zeta, \eta) x_i^{\mathrm{II}} \tag{4}$$

$$y^{\mathrm{II}} = \xi y^{\mathrm{I}} = \sum_{i=1}^{4} \phi_i(\zeta, \eta) y_i^{\mathrm{II}} \tag{5}$$

From Eqs. (4) and (5), both quadrilateral elements II and I could be mapped using the same square shaped master element, which is defined in natural coordinates. In other words, if one isoparametric element has nodal coordinate values similar to the ones of other elements, they are designated as similar elements.

By mapping from the physical coordinates to the natural coordinates, the associated element stiffness matrix $[\boldsymbol{K}]$ for a 2-D elastic problem is then calculated using

$$[\boldsymbol{K}] = \int_{-1}^{1} \int_{-1}^{1} [\boldsymbol{B}]^{\mathrm{T}} [\boldsymbol{D}] [\boldsymbol{B}] \det[\boldsymbol{J}] \, \mathrm{d}\zeta \, \mathrm{d}\eta \tag{6}$$

where

$$[\boldsymbol{B}] = \begin{bmatrix} \dfrac{\partial \phi_i}{\partial x} & 0 & \cdot & \cdot \\ 0 & \dfrac{\partial \phi_i}{\partial y} & \cdot & \cdot \\ \dfrac{\partial \phi_i}{\partial y} & \dfrac{\partial \phi_i}{\partial x} & \cdot & \cdot \end{bmatrix} \tag{7}$$

$$[\boldsymbol{D}] = \frac{E}{1-v^2}\begin{bmatrix} 1 & v & 0 \\ v & 1 & 0 \\ 0 & 0 & \dfrac{1-v}{2} \end{bmatrix} \quad \text{for plane stress} \tag{8}$$

$$[\boldsymbol{D}] = \frac{E}{(1+v)(1-2v)}\begin{bmatrix} 1-v & v & 0 \\ v & 1-v & 0 \\ 0 & 0 & \dfrac{1-v}{2} \end{bmatrix} \quad \text{for plane strain} \tag{9}$$

$$[\boldsymbol{J}] = \begin{bmatrix} \dfrac{\partial x}{\partial \zeta} & \dfrac{\partial y}{\partial \zeta} \\ \dfrac{\partial x}{\partial \eta} & \dfrac{\partial y}{\partial \eta} \end{bmatrix} = \begin{bmatrix} . & . & \dfrac{\partial \phi_i}{\partial \zeta} & . & . \\ . & . & \dfrac{\partial \phi_i}{\partial \eta} & . & . \end{bmatrix} \begin{bmatrix} . & . \\ . & . \\ x_i & y_i \\ . & . \\ . & . \end{bmatrix} \tag{10}$$

Recalling Eq. (1) and from Eqs. (7) and (10), we have

$$[\boldsymbol{B}]^{\mathrm{II}} = \frac{1}{\xi}[\boldsymbol{B}]^{\mathrm{I}} \tag{11}$$

$$\det[\boldsymbol{J}]^{\mathrm{II}} = \xi^2 \det[\boldsymbol{J}]^{\mathrm{I}} \tag{12}$$

Substituting Eqs. (7), (8) and (10) into Eq. (6), it is obvious that

$$[\boldsymbol{K}]^{\mathrm{II}} = [\boldsymbol{K}]^{\mathrm{I}} \tag{13}$$

Eq. (13) indicates the stiffness dimensional independence of similar 2-D isoparametric elements. The development of higher-order elements can be investigated by following the same basic steps.

2.2. Basic infinite element method formulation

The IEM formulation for two-dimensional elasticity problems is presented in this section. The partition concept described in the previous section can be applied to either a perfect body or a body with an imbedded singularity (e.g. crack), as shown in Fig. 2. The meshing steps are described as follows: first, the outer boundary, Γ_0, is properly discretized with the total number of m master nodes, ordered in the counterclockwise direction. Second, by choosing a similar partition center, O, and taking a constant $\xi \in (0,1)$, similar curves $\Gamma_1, \Gamma_2, \ldots, \Gamma_S, \ldots$ of Γ_0 are constructed with center O and proportionality constants $\xi^1, \xi^2, \ldots, \xi^S, \ldots$, respectively. The region bounded between Γ_{i-1} and Γ_i is called the ith element-layer $(i = 1, 2, \ldots, s)$, where s is number of chosen element-layers. Third, each individual Γ_i is regularly discretized like Γ_0, the nodal number and coordinates on each individual Γ_i can be determined from the master node coordinates with geometrically similar conditions. Fourth, every element-layer is auto-meshed into several four-node quadrilateral elements that are similar to one another from the element-layers in a radial direction. The total number of divided elements within one element-layer is m for the perfect domain and $m-1$ is for a cracked domain.

Considering the outermost element-layer, the element stiffness matrix of each quadrilateral element can be calculated and assembled in an element-layer stiffness matrix using the conventional FE formulation. The stiffness matrix of the "first element-layer", can be expressed as suggested in previous studies (Guo, 1979; and Ying, 1992)

$$\begin{bmatrix} \boldsymbol{K_a} & -\boldsymbol{A}^{\mathrm{T}} \\ -\boldsymbol{A} & \boldsymbol{K_b} \end{bmatrix}_{4m\times 4m} \tag{14}$$

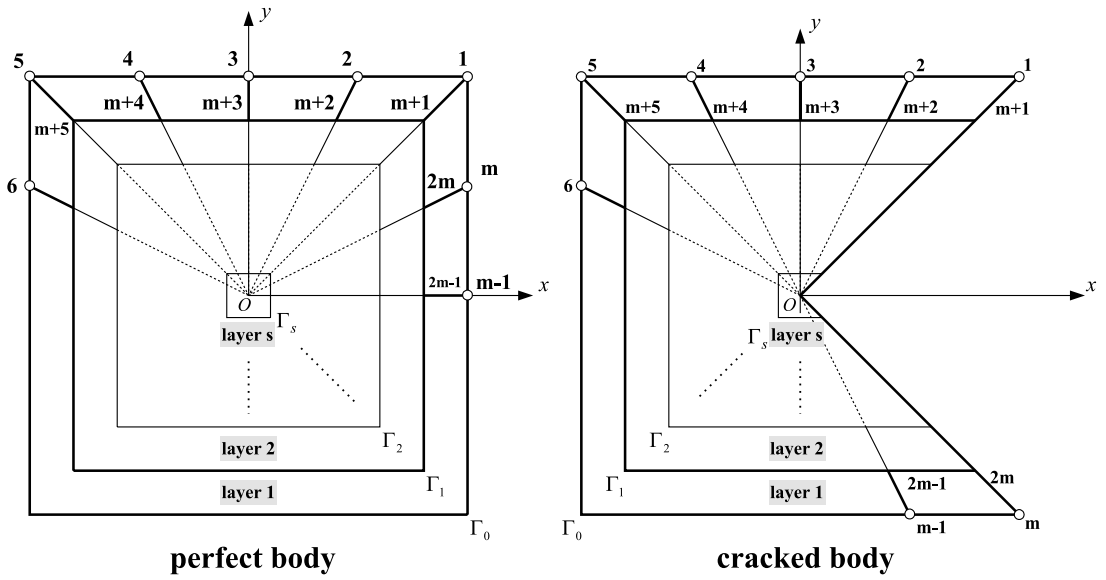

Fig. 2. IE mesh around reference point O.

where $\boldsymbol{K}_a$, $\boldsymbol{K}_b$, and $\boldsymbol{A}$ are the sub-matrices of the stiffness matrix with the same dimension $2m \times 2m$. $\boldsymbol{A}^{\mathrm{T}}$ is the transpose of $\boldsymbol{A}$. Since the global layer stiffness matrix is symmetrical and banded, therefore $\boldsymbol{K}_a$, $\boldsymbol{K}_b$ and $\boldsymbol{A}$ are symmetrical and banded matrices. The nodal displacement vector $\boldsymbol{\delta}_i$ of nodes on Γ_i is defined as

$$\boldsymbol{\delta}_i \equiv \begin{bmatrix} u_1^i & v_1^i & u_2^i & v_2^i & \cdots & u_m^i & v_m^i \end{bmatrix}^{\mathrm{T}} \tag{15}$$

The nodal force vector $\boldsymbol{f}_i$ of nodes on Γ_i is defined as

$$\boldsymbol{f}_i \equiv \begin{bmatrix} f_{1x}^i & f_{1y}^i & f_{2x}^i & f_{2y}^i & \cdots & f_{mx}^i & f_{my}^i \end{bmatrix}^{\mathrm{T}} \tag{16}$$

The ith element-layer stiffness matrix presents the nodal force and displacement vector relationships for Γ_{i-1} and Γ_i. Recalling Eq. (14) and treating the first element-layer as an example, we have

$$\begin{bmatrix} \boldsymbol{K}_a & -\boldsymbol{A}^{\mathrm{T}} \\ -\boldsymbol{A} & \boldsymbol{K}_b \end{bmatrix} \cdot \begin{bmatrix} \boldsymbol{\delta}_0 \\ \boldsymbol{\delta}_1 \end{bmatrix} = \begin{bmatrix} \boldsymbol{f}_0 \\ \boldsymbol{f}_1 \end{bmatrix} \tag{17}$$

Two algebraic equations are extracted from Eq. (17) as follows

$$\boldsymbol{K}_a\boldsymbol{\delta}_0 - \boldsymbol{A}^{\mathrm{T}}\boldsymbol{\delta}_1 = \boldsymbol{f}_0 \tag{18}$$

$$-\boldsymbol{A}\boldsymbol{\delta}_0 + \boldsymbol{K}_b\boldsymbol{\delta}_1 = \boldsymbol{f}_1 \tag{19}$$

where $\boldsymbol{\delta}_0$ and $\boldsymbol{f}_0$ denote the nodal displacements and tractions on Γ_0, respectively. According to the foregoing similarity principle and consequent regular meshing rule, it is obvious that the stiffness matrices of all of the element-layers are the same. Hence we can express the stiffness matrix of the s element-layers (from 1st element-layer to sth element-layer) as a set of algebraic equations, namely

$$\begin{bmatrix} \boldsymbol{K_a} & -\boldsymbol{A}^{\mathrm{T}} \\ -\boldsymbol{A} & \boldsymbol{K_b} \end{bmatrix} \cdot \begin{bmatrix} \boldsymbol{\delta}_0 \\ \boldsymbol{\delta}_1 \end{bmatrix} = \begin{bmatrix} \boldsymbol{f}_0 \\ \boldsymbol{f}_1 \end{bmatrix} \quad \text{for layer 1} \tag{20}$$

$$\begin{bmatrix} \boldsymbol{K_a} & -\boldsymbol{A}^{\mathrm{T}} \\ -\boldsymbol{A} & \boldsymbol{K_b} \end{bmatrix} \cdot \begin{bmatrix} \boldsymbol{\delta}_1 \\ \boldsymbol{\delta}_2 \end{bmatrix} = \begin{bmatrix} -\boldsymbol{f}_1 \\ \boldsymbol{f}_2 \end{bmatrix} \quad \text{for layer 2} \tag{21}$$

$$\begin{bmatrix} \boldsymbol{K_a} & -\boldsymbol{A}^{\mathrm{T}} \\ -\boldsymbol{A} & \boldsymbol{K_b} \end{bmatrix} \cdot \begin{bmatrix} \boldsymbol{\delta}_2 \\ \boldsymbol{\delta}_3 \end{bmatrix} = \begin{bmatrix} -\boldsymbol{f}_2 \\ \boldsymbol{f}_3 \end{bmatrix} \quad \text{for layer 3} \tag{22}$$

$$\vdots$$

$$\begin{bmatrix} \boldsymbol{K_a} & -\boldsymbol{A}^{\mathrm{T}} \\ -\boldsymbol{A} & \boldsymbol{K_b} \end{bmatrix} \cdot \begin{bmatrix} \boldsymbol{\delta}_{s-1} \\ \boldsymbol{\delta}_s \end{bmatrix} = \begin{bmatrix} -\boldsymbol{f}_{s-1} \\ \boldsymbol{f}_s \end{bmatrix} \quad \text{for layer } s \tag{23}$$

Adding the second equation for the ith element-layer and the first equation for the $(i+1)$th element-layer, and letting $\boldsymbol{K} = \boldsymbol{K_a} + \boldsymbol{K_b}$, we have

$$\boldsymbol{K_a}\boldsymbol{\delta}_0 - \boldsymbol{A}^{\mathrm{T}}\boldsymbol{\delta}_1 = \boldsymbol{f}_0 \tag{24}$$

$$-\boldsymbol{A}\boldsymbol{\delta}_0 + \boldsymbol{K}\boldsymbol{\delta}_1 - \boldsymbol{A}^{\mathrm{T}}\boldsymbol{\delta}_2 = 0 \tag{25}$$

$$\vdots$$

$$-\boldsymbol{A}\boldsymbol{\delta}_{i-1} + \boldsymbol{K}\boldsymbol{\delta}_i - \boldsymbol{A}^{\mathrm{T}}\boldsymbol{\delta}_{i+1} = 0 \tag{26}$$

$$\vdots$$

$$-\boldsymbol{A}\boldsymbol{\delta}_{s-2} + \boldsymbol{K}\boldsymbol{\delta}_{s-1} - \boldsymbol{A}^{\mathrm{T}}\boldsymbol{\delta}_s = 0 \tag{27}$$

$$-\boldsymbol{A}\boldsymbol{\delta}_{s-1} + \boldsymbol{K_b}\boldsymbol{\delta}_s = \boldsymbol{f}_s = 0 \tag{28}$$

Let $\boldsymbol{M_S} = \boldsymbol{K_b}$ and substitute it into Eq. (28), we have

$$\boldsymbol{\delta}_s = \boldsymbol{M_S}^{-1}\boldsymbol{A}\boldsymbol{\delta}_{s-1} \tag{29}$$

By substituting Eq. (29) into Eq. (27), we get

$$-\boldsymbol{A}\cdot\boldsymbol{\delta}_{s-2} + (\boldsymbol{K} - \boldsymbol{A}^{\mathrm{T}}\boldsymbol{M_S}^{-1}\boldsymbol{A})\cdot\boldsymbol{\delta}_{s-1} = 0 \tag{30}$$

Comparing Eq. (29) with Eq. (30), two useful iteration formulas can be inferred

$$\boldsymbol{M}_i = \boldsymbol{K} - \boldsymbol{A}^{\mathrm{T}}\boldsymbol{M}_{i+1}^{-1}\boldsymbol{A} \tag{31}$$

$$\boldsymbol{\delta}_i = (\boldsymbol{M}_i^{-1}\boldsymbol{A})\boldsymbol{\delta}_{i-1} = \boldsymbol{X}\boldsymbol{\delta}_{i-1} \tag{32}$$

where $\boldsymbol{X}$ denotes a transfer matrix representing the relationship of $\boldsymbol{\delta}_i$ and $\boldsymbol{\delta}_{i-1}$. Because $\boldsymbol{M_S}$ is known to equal $\boldsymbol{K}_b$, then $\boldsymbol{M}_{S-1}, \boldsymbol{M}_{S-2}, \ldots, \boldsymbol{M}_1$ can be iterated out using Eq. (31). From Eq. (32), we have $\boldsymbol{\delta}_1 = \boldsymbol{M}_1^{-1}\boldsymbol{A}\boldsymbol{\delta}_0$. Substituting $\boldsymbol{\delta}_1$ into Eq. (24), we obtain the most important formula for IEM. That is

$$(\boldsymbol{K_a} - \boldsymbol{A}^{\mathrm{T}}\boldsymbol{M}_1^{-1}\boldsymbol{A})\cdot\boldsymbol{\delta}_0 = \boldsymbol{K_Z}\cdot\boldsymbol{\delta}_0 = \boldsymbol{f}_0 \tag{33}$$

where $\boldsymbol{K_Z} = (\boldsymbol{K_a} - \boldsymbol{A}^{\mathrm{T}}\boldsymbol{M}_1^{-1}\boldsymbol{A})$ is called the combined element stiffness matrix which preserves the symmetry characteristic of global stiffness matrix in FE standard procedures. Once $\boldsymbol{f}_0$ (the outer surface traction) is given, $\boldsymbol{\delta}_0$ can be obtained from Eq. (33). Then $\boldsymbol{\delta}_1, \boldsymbol{\delta}_2, \ldots, \boldsymbol{\delta}_s$ can be found sequentially from Eq. (32). Using the procedure from Eq. (24) to (28); adding layer by layer, all of the inner layer elements are condensed and transformed into only one super-element with master nodes at the outer boundary Γ_0 only. This is called

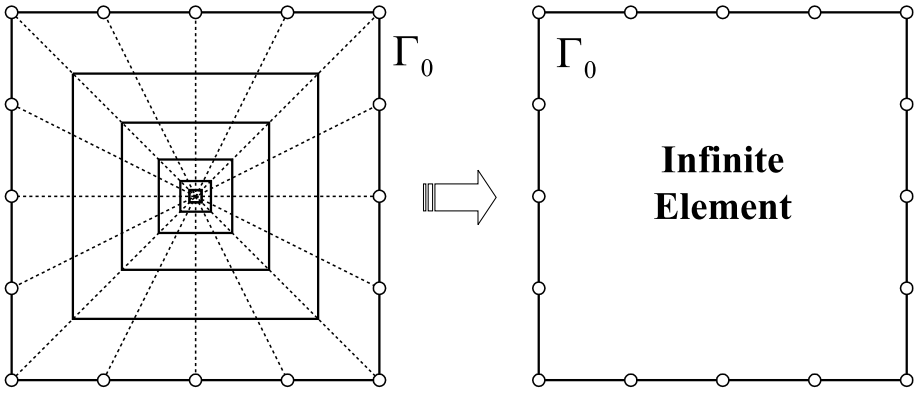

Fig. 3. Schematic diagram of IE formation.

the IE, as shown in Fig. 3. Consequently the IE can be with arbitrary configuration and arbitrary number of master nodes. From the physical point of view, we treat the $\boldsymbol{K}_{\boldsymbol{Z}}$ term as the equivalent stiffness matrix of the IE with a dimension of $2m \times 2m$. Although the total degree of freedom of $\boldsymbol{K}_{\boldsymbol{Z}}$ is largely reduced, the mesh refinement effect of large amounts of infinitesimal elements around the singular point is maintained and does not increase any corresponding round-off errors because of its specific matrix condensation process. Moreover, to compute $\boldsymbol{K}_{\boldsymbol{Z}}$, only to calculate the outermost element-layer stiffness matrix with the chosen ξ proportion ratio and element-layer number s is need. The CPU time and PC memory storage are also significantly reduced.

Prior to applying the newly defined IE for further numerical analysis, a detailed convergence study involving the IE stiffness matrix, $\boldsymbol{K}_{\boldsymbol{Z}}$, should be considered. Whether the stiffness matrix is convergent or not depends primarily on the number of layers selected in the IEM formulation. Ying (1992) proved that $\boldsymbol{K}_{\boldsymbol{Z}}$ is a semi-positive definite matrix that converges at a certain constant quantity when the number of layers approach infinity. This can be expressed in the following form:

$$\lim_{s\to\infty} \boldsymbol{K}_{\boldsymbol{Z}}^{(s)} = \boldsymbol{K}_{\boldsymbol{Z}} \tag{34}$$

where s denotes the number of chosen element-layers. Eq. (34) cannot be directly applied to the numerical formulation because the term "infinite" is not countable in a physical sense. However, if s is a large enough finite number, the stiffness matrix $\boldsymbol{K}_{\boldsymbol{Z}}^{(s)}$ is approximately equal to $\boldsymbol{K}_{\boldsymbol{Z}}$. Therefore, we propose observing the convergence of the diagonal trace terms $\boldsymbol{K}_{\boldsymbol{Z}}^{(s)}(j,j)$. If the first invariant of $\boldsymbol{K}_{\boldsymbol{Z}}^{(s)}$, which is used as the criterion to make sure $\boldsymbol{K}_{\boldsymbol{Z}}^{(s)}$ is close enough to $\boldsymbol{K}_{\boldsymbol{Z}}$, an iterative scheme is established based on the above concept and a sequence of $\boldsymbol{K}_{\boldsymbol{Z}}(j,j)$ can be obtained. When the desired accuracy criterion $\varepsilon = |(\boldsymbol{K}_{\boldsymbol{Z}}^{(i+1)}(j,j) - \boldsymbol{K}_{\boldsymbol{Z}}^{(i)}(j,j))|/|(\boldsymbol{K}_{\boldsymbol{Z}}^{(i+1)}(j,j))| \times 100\% \leqslant 10^{-6}$ is satisfied, the iterative process is terminated and the critical number of element-layers, "s_{cr}", is determined as equal to the terminated iterative value of j. This denotes the minimum number of element-layers needed for convergence. The above method is the criterion for checking the convergence of $\boldsymbol{K}_{\boldsymbol{Z}}$. Once s is greater than or equal to s_{cr}, $\boldsymbol{K}_{\boldsymbol{Z}}$ converges. This implies that there are enough elements to cover the entire problem domain. Though a tiny void exists, it can be neglected because it does not affect $\boldsymbol{K}_{\boldsymbol{Z}}$. Conversely, if s is smaller than s_{cr}, a small void actually exists in the domain and it cannot be neglected.

Another important factor also considered in the convergence study is the proportionality ratio ξ. Intuitively, it is believed that the greater the chosen ξ, the more s_{cr} is needed. Variations in ξ do not change the amount of computational works but does affect the resulting numerical solution. The detailed discussion on this is postponed until Example 3 in Section 3.

2.3. Infinite element–finite element coupling method

When the problem includes multiple cracks, using IEM to model the entire domain is not favorable. Therefore an IEM/FEM coupled scheme is proposed using IE to sub-divide the neighborhood of each crack. Outside the singular IE sub-domains, the solutions are obtained using the conventional FEM. The master nodes on the outer boundary at each IE are converted into interface nodes between the IE and FE sub-domains. Because each IE stiffness matrix is pre-determined, those elements can be treated as regular FEs to be assembled into the global stiffness matrix formed using FEM.

To illustrate the coupling algorithm, a single crack body is shown in Fig. 4 that can be partitioned into two sub-domains, Ω and D, separated from the coupling interface, Γ_0, and modeled using the FEM and IEM, respectively. The algebraic assembled element equations for the FE sub-domain are given by the well-known FE implementation (Kwon and Bang, 2000)

$$\boldsymbol{K}\boldsymbol{\delta} = \boldsymbol{F} \tag{35}$$

where $\boldsymbol{K}$ is the global stiffness matrix of the FE sub-domain and $\boldsymbol{F}$ and $\boldsymbol{\delta}$ are the nodal forces and nodal displacements, respectively. Furthermore, Eq. (35) can be written as

$$\begin{bmatrix} \boldsymbol{K}_{\text{couple}} & \boldsymbol{K}_{\text{cf}}^{\text{T}} \\ \boldsymbol{K}_{\text{cf}} & \boldsymbol{K}_{\text{fem}} \end{bmatrix} \cdot \begin{bmatrix} \boldsymbol{\delta}_0 \\ \boldsymbol{\delta}_{\text{fem}} \end{bmatrix} = \begin{bmatrix} \boldsymbol{F}_{0\,\text{fem}} \\ \boldsymbol{F}_{\text{fem}} \end{bmatrix} \tag{36}$$

where $\boldsymbol{\delta}_0$ and $\boldsymbol{\delta}_{\text{fem}}$ denote the vectors of the IE/FE interface and non-interface nodal displacements, respectively. $\boldsymbol{F}_{0\,\text{fem}}$ and $\boldsymbol{F}_{\text{fem}}$ are the associated loading vectors, respectively. From Eq. (36), the two equations are extracted as

$$\boldsymbol{K}_{\text{couple}}\boldsymbol{\delta}_0 + \boldsymbol{K}_{\text{cf}}^{\text{T}}\boldsymbol{\delta}_{\text{fem}} = \boldsymbol{F}_{0\,\text{fem}} \tag{37}$$

$$\boldsymbol{K}_{\text{cf}}\boldsymbol{\delta}_0 + \boldsymbol{K}_{\text{fem}}\boldsymbol{\delta}_{\text{fem}} = \boldsymbol{F}_{\text{fem}} \tag{38}$$

Conversely, the IE sub-domain produces the following algebraic equation using the IEM described in detail in the previous section

$$\boldsymbol{K}_{\text{IEM}}\boldsymbol{\delta}_0 = \boldsymbol{F}_{0\,\text{iem}} \tag{39}$$

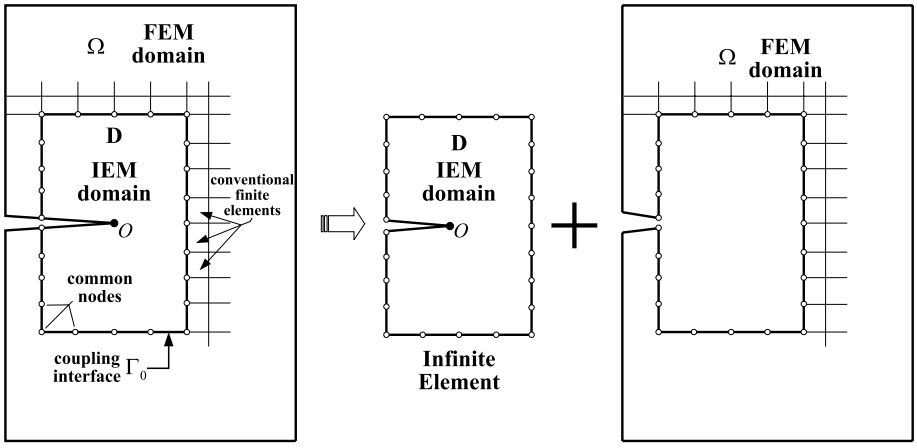

Fig. 4. Schematic diagram of IE–FE coupling method.

where $\boldsymbol{K}_{\mathrm{IEM}} = \boldsymbol{K}_{\boldsymbol{Z}} = (\boldsymbol{K}_{\boldsymbol{a}} - \boldsymbol{A}^{\mathrm{T}}\boldsymbol{M}_1^{-1}\boldsymbol{A})$, denotes the combined stiffness matrix $\boldsymbol{K}_{\boldsymbol{Z}}$ of the IE sub-domain. $\boldsymbol{\delta}_0$ and $\boldsymbol{F}_{0\,\mathrm{iem}}$ denote the interface displacements and the associated loading vectors, respectively.

Along the IE/FE interface, the displacement compatibility and force equilibrium must be satisfied. Thus Eqs. (37) and (39) are combined and we have

$$(\boldsymbol{K}_{\mathrm{couple}} + \boldsymbol{K}_{\mathrm{IEM}})\boldsymbol{\delta}_0 + \boldsymbol{K}_{\mathrm{cf}}^{\mathrm{T}}\boldsymbol{\delta}_{\mathrm{fem}} = \boldsymbol{F}_{0\,\mathrm{iem}} + \boldsymbol{F}_{0\,\mathrm{fem}} = 0 \tag{40}$$

Eqs. (38) and (40) are combined to give the IE–FE final coupled equation of the form:

$$\begin{bmatrix} \boldsymbol{K}_{\mathrm{couple}} + \boldsymbol{K}_{\mathrm{IEM}} & \boldsymbol{K}_{\mathrm{cf}}^{\mathrm{T}} \\ \boldsymbol{K}_{\mathrm{cf}} & \boldsymbol{K}_{\mathrm{fem}} \end{bmatrix} \cdot \begin{bmatrix} \boldsymbol{\delta}_0 \\ \boldsymbol{\delta}_{\mathrm{fem}} \end{bmatrix} = [\boldsymbol{K}_{\mathrm{IE-FE}}] \cdot \begin{bmatrix} \boldsymbol{\delta}_0 \\ \boldsymbol{\delta}_{\mathrm{fem}} \end{bmatrix} = \begin{bmatrix} 0 \\ \boldsymbol{F}_{\mathrm{fem}} \end{bmatrix} \tag{41}$$

It is apparent that the corresponding coupled system stiffness matrix $[\boldsymbol{K}_{\mathrm{IE-FE}}]$ is a symmetrical matrix. Displacements in the FE sub-domain can be obtained by solving Eq. (41). Once we obtain the interface nodal displacements $\boldsymbol{\delta}_0$, the traction along IE/FE interface $\boldsymbol{F}_{0\,\mathrm{iem}}$ can be found by solving Eq. (39), and the nodal displacement at each node in the IE sub-domain can be obtained using Eq. (32).

For multiple crack problems, all crack tips can be modeled using the IE, which are then assembled into the global stiffness matrix formed from the FE sub-domain. Because the similar element concept is extended, all crack tips with similar IE sub-domains have the same stiffness matrix. Calculating only one of the IE stiffness matrices is enough for all the others. This technique greatly reduces the computational cost and work in modeling the required mesh for cracks.

2.4. Calculation of stress intensity factor

Other important quantities such as the K, G, and J-integral in the IE sub-domain can be obtained for the FE representation. A polar coordinate axis with the origin at the crack tip, namely r and θ, is defined and shown in Fig. 5. The mode I crack tip stress intensity factor (SIF) K_{I} can then be estimated using the established crack tip relations. The K_{I} corresponding to the y-directional displacement along the crack surface (U_y) is approximated using (Chan et al., 1970)

$$K_{\mathrm{I}} = \frac{E}{8C}\lim_{r\to 0}\sqrt{\frac{2\pi}{r}}\left[U_y(r)^{\theta=180^\circ} - U_y(r)^{\theta=-180^\circ}\right] \tag{42}$$

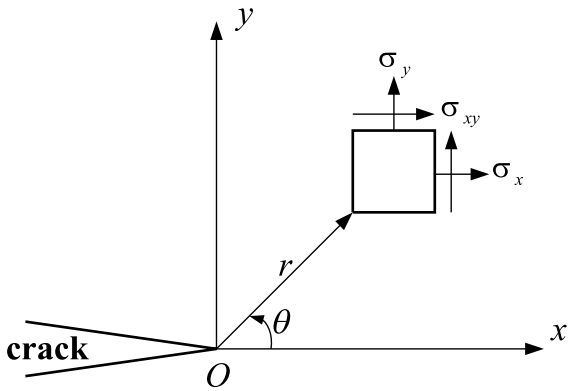

Fig. 5. Definition of the coordinate system ahead of a crack tip.

where $C = 1$ is used for the plane stress condition and $C = 1 - v^2$ is used for the plane strain condition. E, v, and r indicate Young's modulus, Poisson's ratio, and the distance from the crack tip for picked nodal points, respectively.

3. Numerical examples

In this section, six examples are presented to demonstrate the validity of the results obtained using the proposed IEM and IEM/FEM formulation. The related programs used in this study were programmed in the MATLAB v.5.3 language and operated on a P-III personal computer. The first simple elasticity problem is presented to verify the developed IEM codes. The second and third examples are applied using the IEM and IEM/FEM codes to solve the center crack tension (CCT) problem and compare the solution accuracy with the analytical solutions. An extended study for oblique edge crack problem is presented in the fourth example. The fifth and sixth examples are applied using the IEM/FEM codes to calculate SIF for a strip with four parallel center-through-cracks and a trip with two collinear cracks to demonstrate the ability of the IE–FE coupling algorithm to solve multiple crack problems.

Example 1. A plate subjected to uniform compressive stress on two free ends

Consider a thin rectangular plate with panel dimensions (400 mm × 200 mm) as shown in Fig. 6. The elastic modulus and Poisson's ratio are $E = 70{,}000$ N/mm^2, $v = 0.3$, respectively. A uniform compressive stress P of 400 N/mm^2 is acted at the two free ends. The points along $\overline{AB}$ and $\overline{CD}$ move along x-direction and are constrained in the y-direction. The analytical displacement fields under plane stress condition for points along $\overline{AB}$ and $\overline{CD}$ are expressed as

$$u = -\frac{1 - v^2}{E} P \cdot x \tag{43}$$

$$v = 0 \tag{44}$$

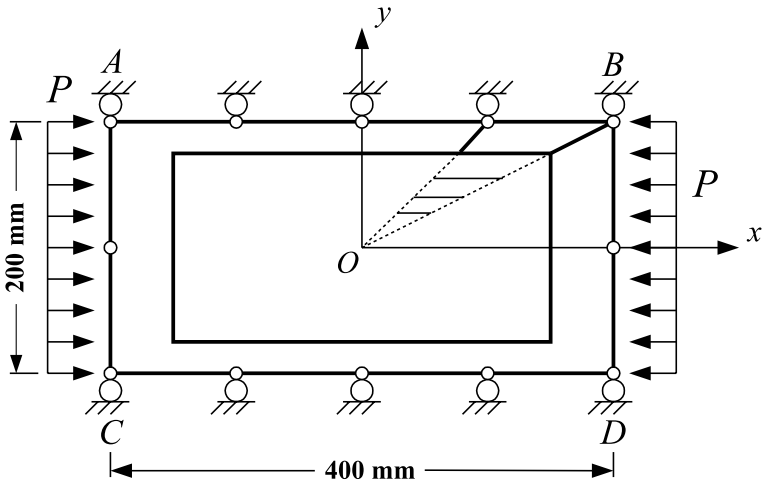

Fig. 6. Computational model of a plate under compressive stress on two free ends.

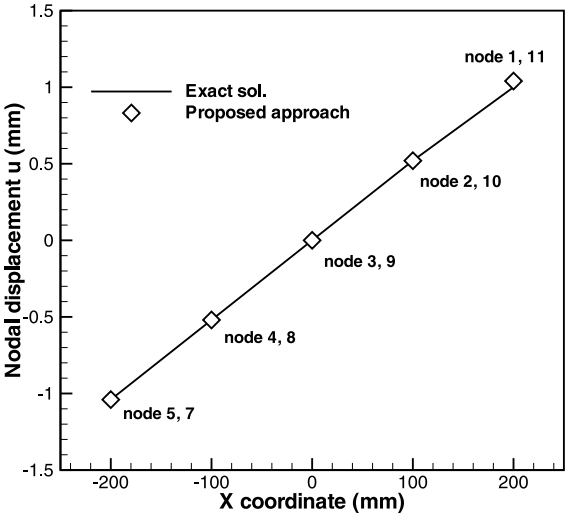

Fig. 7. Comparisons between proposed approach and analytical solution of displacement u along $\overline{AB}$ and $\overline{CD}$ shown in Fig. 6.

The mesh configuration and node arrangement are shown in Fig. 6. The graph comparing the nodal displacement field from the theoretical solution and the present IEM solution is shown in Fig. 7. The results are shown to be in very good agreement.

Example 2. Center crack tension (CCT) problem

Consider a strip with a center through crack $2a$ and finite width w a subjected to a uniform tensile stress σ, as shown in Fig. 8. The mesh configuration and node arrangement are the same shown in the figure. Because of the geometric symmetry and the load type, only half of the full strip, with the load and boundary conditions as shown, need be addressed. A total of 25 master nodes exist, uniformly distributed along the circumferential directions along boundary Γ_0. The proportionality ratio ξ is selected as 0.9 to calculate the stiffness matrix of $\boldsymbol{K}_{\mathrm{IEM}}$.

The analytical expression for the mode I SIF for CCT is expressed as

$$\boldsymbol{K}_{\mathrm{I}} = \sigma\sqrt{(\pi a)}f(a/w) \tag{45}$$

where the factor $f(a/w)$ is a function of the crack length a and the strip width w. The factor is found as follows (Marc and Krishan, 1999)

$$f(a/w) = 1 + 0.256(a/w) - 1.152(a/w)^2 + 12.2(a/w)^3 \tag{46}$$

Fig. 9 represents comparison of the results for the normalized mode I SIF $K_{\mathrm{I}}/\sigma\sqrt{\pi a}$ against the (a/w) ratio obtained from the IEM approach, with the analytical solutions from Eqs. (45) and (46). The numerical, analytical data and relative difference (RD) estimate are provided in Table 1. Both the numerical and analytical results are in good agreement. The maximum difference is less than 5%.

Example 3. IE–FE Coupling method in center crack tension problem

Fig. 10 shows the IEM/FEM coupled computational model of a strip, where D represents the IE sub-domain, and Ω represents the FE sub-domain. A total of 25 master nodes are uniformly distributed along

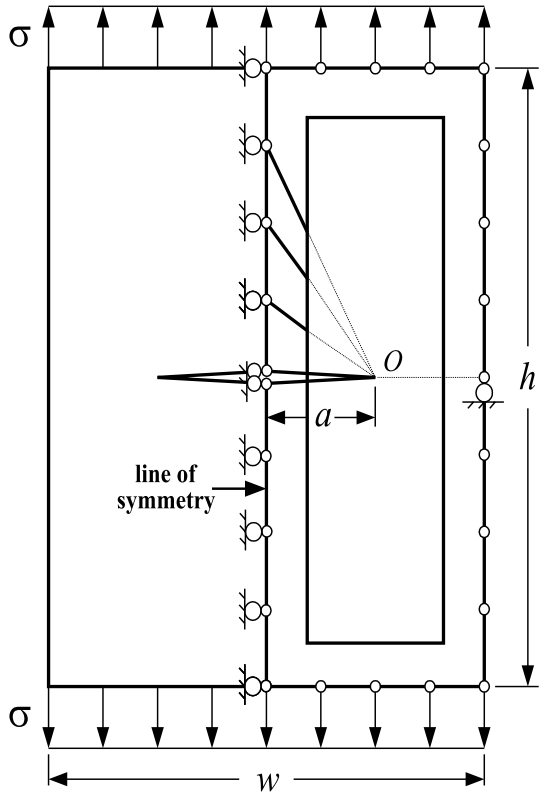

Fig. 8. IEM computational model of CCT problem.

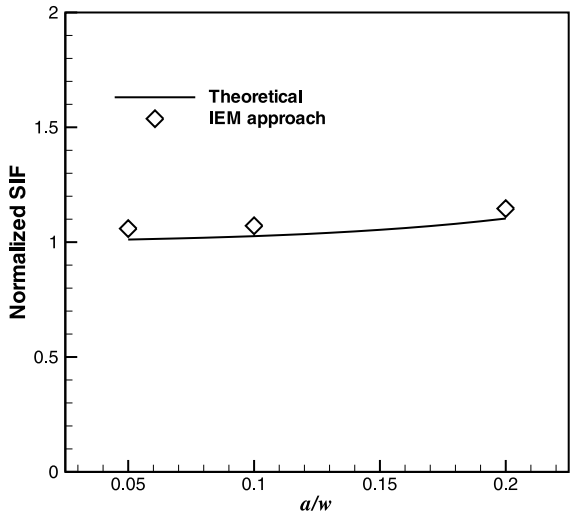

Fig. 9. Normalized SIF for CCT by IEM.

Table 1
Normalized SIF of CCT by IEM

a/w	$K_I/\sigma\sqrt{\pi a}$ ($\xi = 0.9$)		
	Present	RD (%)	Theoretical
0.05	1.059084	4.71	1.01145
0.1	1.071472	4.40	1.02628
0.2	1.146188	3.94	1.10272

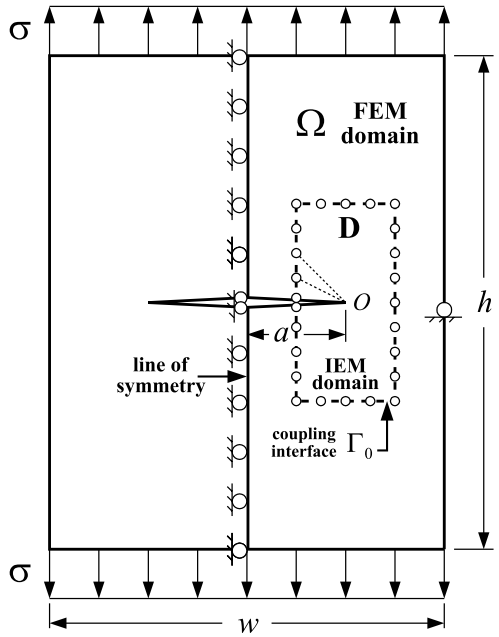

Fig. 10. IE–FE coupling computational model of CCT problem.

the circumferential directions along the coupling interface Γ_0 to form the IE. The proportionality ratio ξ is selected as 0.9 to calculate the IE stiffness matrix of $\boldsymbol{K}_{\mathrm{IEM}}$, which then is assembled into a global system stiffness matrix for the FE sub-domain Ω using IE–FE coupling algorithm. One can easily solve for $\boldsymbol{\delta}_0$ from Eq. (41), and consequently follow the same procedures as in Example 2 to obtain the mode I SIF for the crack.

The normalized mode I SIF $\boldsymbol{K}_I/\sigma\sqrt{\pi a}$ against the (a/w) ratio is plotted in Fig. 11. The numerical, analytical data and RD estimate are tabulated in Table 2. Good agreement with analytical solution was obtained. Compared with Example 2, the results obtained using IE–FE coupling method were significantly improved. The RD was less than 1%.

A parameter study of the various proportionality ratios ξ using the IE–FE coupling method was also investigated. The results are given in Table 3. It is clear that subsequently decreasing ξ to 0.5 leads to increasing the RD not more than 2.1%. Increasing ξ up to 0.95 does not significantly affect the results.

Example 4. IE–FE coupling method in slant edge crack problem

The identical application of the IE–FE coupling method described in Example 3 has been used to investigate the normalized mode I SIF for oblique cracks with different slant angles and crack lengths.

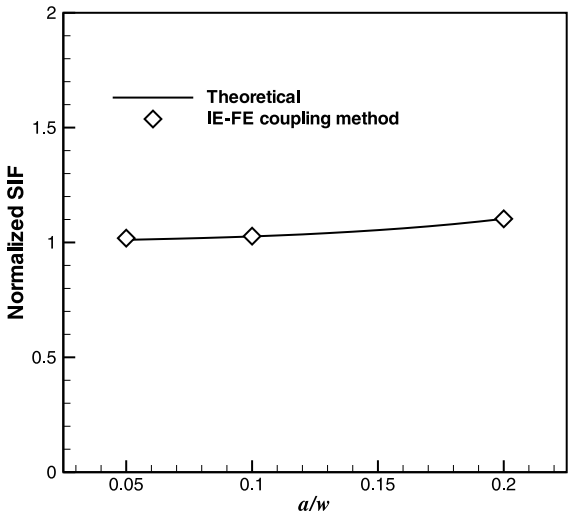

Fig. 11. Normalized SIF for CCT by IE–FE coupling method.

Table 2
Normalized SIF of CCT by IE–FE coupling method

a/w	$K_I/\sigma\sqrt{\pi a}$ ($\xi = 0.9$)		
	Present	RD (%)	Theoretical
0.05	1.018672	0.71	1.01145
0.1	1.027433	0.11	1.02628
0.2	1.102886	0.01	1.10272

Table 3
Normalized SIF of CCT by IE–FE coupling method in variation of proportionality ratios ξ ($a/w = 0.05$)

ξ	$K_I/\sigma\sqrt{\pi a}$	
	Present	RD (%)
0.5	1.032780	2.10
0.6	1.027602	1.60
0.7	1.022602	1.10
0.8	1.020095	0.85
0.9	1.018672	0.71
0.95	1.018405	0.69
Theoretical	1.011450	

Consider an oblique edge crack of length a in a finite rectangular strip of width w and length $2.5b$ ($b = w$) as shown in Fig. 12, subjected to a uniform tensile stress σ on the strip ends. As already mentioned, D represents the IE sub-domain, and Ω represents the FE sub-domain. A total of 57 master nodes are uniformly distributed along the coupling interface Γ_0. This geometric configuration is selected since it has been analyzed by Leung and Su (1995). The crack makes an angle β on the long edge of the strip. Two geometric factors, for $\beta = 90°$, 67.5° and 45° and for $a/w = 0.2$, 0.3, 0.4, 0.5, and 0.6 have been considered. Fig. 13 represents the comparison of the results for the normalized mode I SIF for various values of β and a/w obtained from the IE–FE coupling approach, with the results of Leung and Su (1995). The results from both methods agree well.

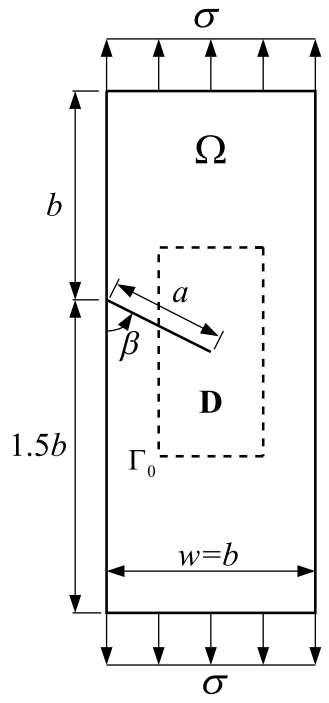

Fig. 12. IE–FE coupling computational model of slant edge crack problem.

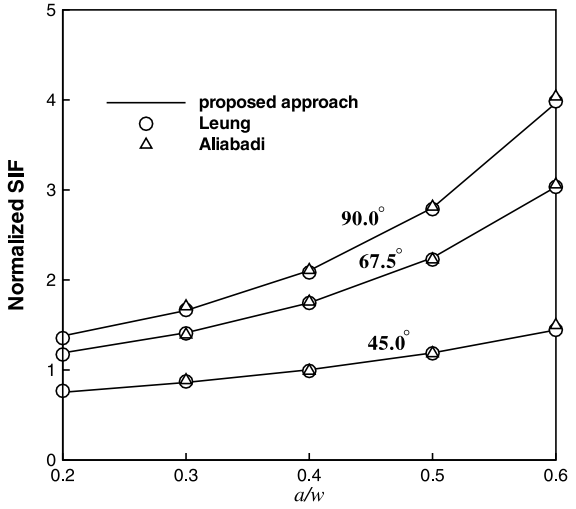

Fig. 13. Mode I SIF for slant edge crack problem.

Example 5. IE–FE coupling method in parallel internal cracks problem

Consider a strip with a row of four parallel center-through-cracks $2a$ subjected to uniform tensile stress σ, as shown in Fig. 14. The spacing between the cracks is d. The schematic mesh configuration in the strip

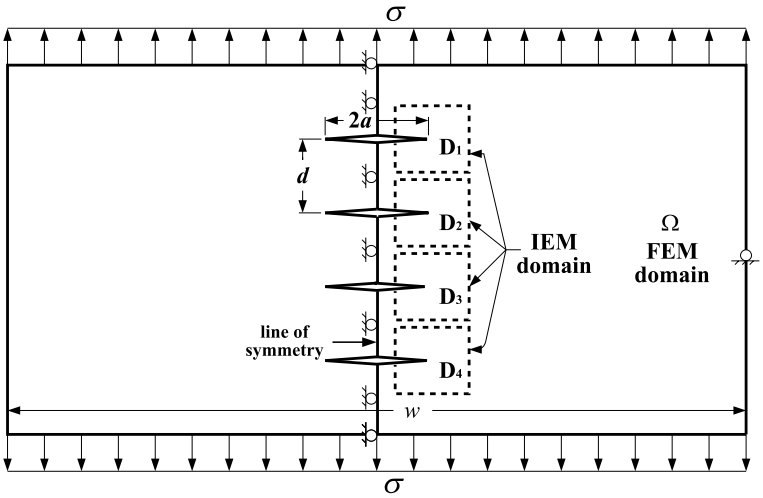

Fig. 14. IE–FE coupling computational model of four parallel center cracks problem.

is the same as shown in the figure. Four identical IE sub-domains D_1, D_2, D_3, and D_4 are generated around the crack tips to form four IE. The proportionality ratio ξ is selected as 0.9 to calculate the IE stiffness matrix of $\boldsymbol{K}_{\mathrm{IEM}}$. Based on the similar partition property of two-dimensional isoparametric elements described in Section 2.1, all of the IE have an identical stiffness matrix. Therefore only one of the IEs, say $\boldsymbol{K}_{\mathrm{IEM}}$ at D_1 need to be calculated. After IEM formulation, four IEs with the same stiffness matrix are then assembled into a global stiffness matrix formed in the FE sub-domain Ω. Following the same approach as in Example 3, we can obtain SIF for each crack.

Since no closed-form solution for this example, we only can compare numerical results with the analytical solution of an infinite long strip with periodically parallel-arranged and equally-spaced cracks. The analytical expression for the mode I SIF can be expressed as (Menčík, 1992)

$$K_{\mathrm{I}} = \sigma\sqrt{(\pi a)}f(a/d) \quad \text{for } 2a \ll w \tag{47}$$

where the $f(a/d)$ factor characterizes the effect of the crack length to crack spacing ratio. This factor is found as follows

$$f(a/d) = \mathrm{e}^{-1.68q} \cdot (1 + 1.68q) \tag{48}$$

where $q = 2a/d$ and it was chosen as 0.2 in this example. The RD estimate of the normalized mode I SIF $K_{\mathrm{I}}/\sigma\sqrt{\pi a}$ for cracks at D_1 and D_2 is listed in Table 4. The result obtained from D_2 agrees well with the analytical solution with as little difference as 1.91%. The result obtained from D_1 is slightly larger because the crack in D_1 is near the load end. It can be expected that the damage and failure of the strip with parallel-arranged and equally-spaced cracks would first initiate at the tips of the deviating cracks.

Table 4
Normalized SIF of four parallel center cracks problem

IEM domain	$K_{\mathrm{I}}/\sigma\sqrt{\pi a}$ ($\xi = 0.9, 2a/d = 0.2$)		
	Present	RD (%)	Theoretical
D_1	0.99946	4.68	0.954736
D_2	0.97296	1.91	0.954736

Example 6. IE–FE coupling method in collinear internal cracks problem

Consider a rectangular plate with two collinear cracks of equal length, $2a$, under uniform tensile stress, as shown in Fig. 15. The geometric factors of the cracked plate, crack-spacing-to-width ratio ($e/b = 0.5$), four height-to-width ratios ($c/b = 1.5, 1, 0.75, 0.5$) and three crack-length-to-width ratios ($a/e = 0.4, 0.5, 0.6$) are taken into consideration. Four IE sub-domains of D_1, D_2, D_3, and D_4 are generated to form four IEs around four crack tips of the two collinear cracks. The region Ω outside the IE sub-domains is modeled using FEM. A total of 51 master nodes exist, uniformly distributed along the boundary of each IEM sub-domain. In D_1, D_2, D_3, and D_4, the proportionality ratio ξ is selected as 0.9 with respect to the related crack tip as their similar partition center. Based on the similar partition property, only two IE stiffness matrices, say $\boldsymbol{K}_{D_1}$ and $\boldsymbol{K}_{D_2}$ at D_1 and D_2, need to be calculated and they accurately represent the other two IE stiffness matrices of $\boldsymbol{K}_{D_3}$ and $\boldsymbol{K}_{D_4}$ at D_3 and D_4, respectively. In MATLAB programming, the geometric factor of the crack-length-to-width ratio is parameterized so that it is very easy to adjust crack length by varying the coordinate value of the crack tip.

The normalized mode I SIF at crack tips A and B, as shown in Fig 15, for the different divided cases are calculated and the numerical results are listed in Tables 5–7 in comparison with those of Wang (1997). When compared with those by Wang, who uses the boundary force method, good agreements are obtained. The RD of our results stays within 4% of the Wang's solution. It is clear that subsequently increasing the crack-length-to-width ratio and decreasing the height-to-width ratio of the plate would lead to increasing the SIF.

The above two examples illustrate that the proposed IEM/FEM coupled method is highly efficient and accurate enough to be used for solving elastic multiple crack problems.

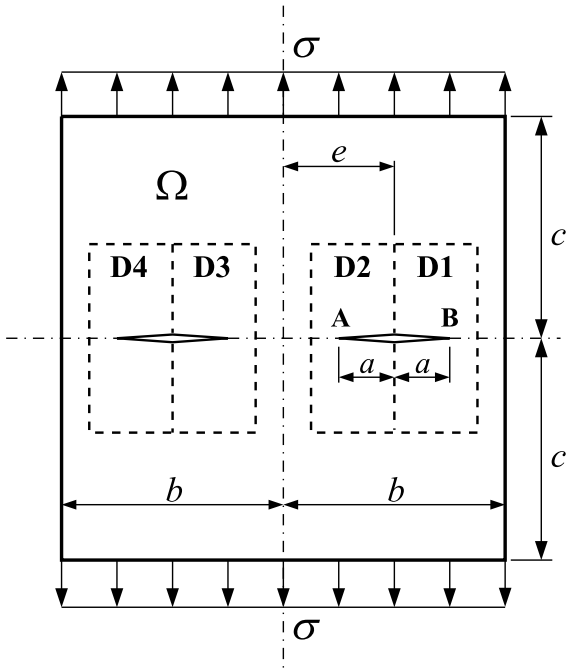

Fig. 15. IE–FE coupling computational model of two collinear cracks problem.

Table 5
Normalized SIF of two collinear cracks problem in the case of $a/e = 0.4$

c/b	F_{I}	$a/e = 0.4$		
		Ref.	Present	RD (%)
1.5	F_{IA}	1.0930	1.0998	0.62
	F_{IB}	1.0960	1.1009	0.45
1.0	F_{IA}	1.0967	1.0994	0.25
	F_{IB}	1.0955	1.0967	0.11
0.75	F_{IA}	1.1076	1.1097	0.19
	F_{IB}	1.1013	1.1021	0.07
0.5	F_{IA}	1.1678	1.1872	1.66
	F_{IB}	1.1714	1.1896	1.55

$F_{\mathrm{IA}} = \dfrac{K_{\mathrm{IA}}}{\sigma\sqrt{\pi a}}$; $F_{\mathrm{IB}} = \dfrac{K_{\mathrm{IB}}}{\sigma\sqrt{\pi a}}$.

Table 6
Normalized SIF of two collinear cracks problem in the case of $a/e = 0.5$

c/b	F_I	$a/e = 0.5$		
		Ref.	Present	RD (%)
1.5	F_{IA}	1.1573	1.1429	1.24
	F_{IB}	1.1630	1.1457	1.49
1.0	F_{IA}	1.1633	1.1574	0.51
	F_{IB}	1.1610	1.1526	0.72
0.75	F_{IA}	1.1792	1.1767	0.21
	F_{IB}	1.1664	1.1617	0.40
0.5	F_{IA}	1.2562	1.2850	2.29
	F_{IB}	1.2584	1.2879	2.34

Table 7
Normalized SIF of two collinear cracks problem in the case of $a/e = 0.6$

c/b	F_{I}	$a/e = 0.6$		
		Ref.	Present	RD (%)
1.5	F_{IA}	1.2535	1.2191	2.74
	F_{IB}	1.2632	1.2236	3.14
1.0	F_{IA}	1.2626	1.2469	1.24
	F_{IB}	1.2587	1.2387	1.59
0.75	F_{IA}	1.2837	1.2748	0.69
	F_{IB}	1.2609	1.2484	0.99
0.5	F_{IA}	1.3697	1.4060	2.65
	F_{IB}	1.3629	1.4066	3.20

4. Conclusion

An elegant IE–FE coupling algorithm was demonstrated to provide highly accurate numerical solutions for two-dimensional multiple crack problems. This method is equally well suited for the usual regularity closed domain and other types of singularities; e.g. re-entrant corners, dissimilar material junctions. Based on the similarity partition concept for isoparametric elements along with the IEM formulation, great numbers of infinitesimal elements are automatically generated layer by layer around the singularity point in each IE sub-domain. All of the d.o.f.'s in the IE sub-domain, except for those associated with the coupling interface, are condensed and transformed to form a so-called "Infinite Element IE" with master nodes only. We also proposed the convergence criterion for obtaining the countable "infinite layers", s_{cr}, which assures that $\boldsymbol{K}_{\boldsymbol{Z}}$ is convergent. All of the IEs are treated as regular FEs and their stiffness matrices are assembled into the system stiffness matrix for the FE sub-domain. The resultant FE solution with a symmetrical stiffness matrix, having the singularity effect of imbedded cracks in IEs, is required only for solving multiple crack problems. No prior governing assumption is required and no special FEs, such as singular, hybrid and boundary elements need be incorporated. No further parametric refinement analysis is needed because of the high IEM formulation convergence. The corresponding round-off errors, CPU time, and PC memory storage on these computations are also significantly reduced.

The numerical examples given in this paper validated and illustrated the proposed methodology. Good agreements were obtained between the known results and the proposed method. A parameter study of the various proportionality ratios is also conducted. From the numerical example, a proportionality ratio ξ equal to 0.9 can obtain very good numerical results. Decreasing ξ lower to 0.5 still obtains reasonable results from the proposed method.

Acknowledgements

The authors would like to thank the National Science Council, Taiwan, R.O.C., for financially supporting this research under grant NSC88-2212-E-194-010. Professor C.F. Lee at the Department of Engineering Science, National Cheng Kung University in Taiwan is acknowledged for his helpful inputs during this research.

References

Ang, W.T., Clements, D.L., 1995. Hypersingular integral equations for multiple interacting planar cracks in an elastic layered material under antiplane shear stresses. Engineering Analysis with Boundary Elements 16, 289–295.

Barut, A., Guven, I., Madenci, E., 2001. Analysis of singular stress fields at junctions of multiple dissimilar materials under mechanical and thermal loading. International Journal of Solids and Structures 38, 9077–9109.

Bois-Grossiant, P., Tan, C.L., 1995. Boundary element fracture mechanics analysis of Brazil-nut sandwich specimens with an interface crack. Engineering Analysis with Boundary Elements 16, 215–225.

Buettner, A.D., Quesnel, D.J., 1993. Calculation of stress intensity using multimesh extrapolation. Finite Elements in Analysis and Design 14, 325–336.

Burczynski, T., Beluch, W., 2001. The identification of cracks using boundary elements and evolutionary algorithms. Engineering Analysis with Boundary Elements 25, 313–322.

Chan, S.K., Tuba, I.S., Wilson, W.K., 1970. On the finite element method in linear fracture mechanics. Engineering Fracture Mechanics 2, 1–17.

Chow, W.T., Beom, H.G., Atluri, S.N., 1995. Calculation of stress intensity factors for an interfacial crack between dissimilar anisotropic media, using a hybrid element method and the mutual integral. Computational Mechanics 15, 546–557.

Cruse, T.A., 1988. Boundary Element Analysis in Computational Fracture Mechanics. Kluwer Academic Publishers, The Netherlands.

Go, C.G., Lin, Y.S., 1991. Infinitely small element for the problem of stress singularity. Computers & Structures 37 (4), 547–551.

Go, C.G., Chen, G.C., 1992. On the use of an infinitely small element for the three-dimensional problem of stress singularity. Computers & Structures 45 (1), 25–30.

Guo, Z.H., 1979. Similar isoparametric elements. Science Bulletin 24 (13), 577–582.

Han, H.D., Ying, L.A., 1979. An iterative method in the finite element. Mathematica Numerica Sinica 1 (1), 91–99.

Hasebe, N., Qian, J., Chen, Y., 1996. Fundamental solutions for half plane with an oblique edge crack. Engineering Analysis with Boundary Elements 17, 263–267.

Her, S.C., 2000. Fracture analysis of interfacial crack by global–local finite element. International Journal of Fracture 106, 177–193.

Kang, C.H., De Saxcé, G., 1992. Computation of stress intensity factors for plate bending problem in fracture mechanics by hybrid mongrel finite element. Computers & Structures 42 (4), 581–589.

Katsareas, D., Anifantis, N., 1995. Boundary element analysis of thermally stressed interface cracks. Engineering Fracture Mechanics 50 (1), 51–60.

Kermanidis, Th.B., Mavrothanasis, F.I., 1995. Calculation of mode III stress intensity factor by BEM for cracked axisymmetric bodies. Computational Mechanics 16, 124–131.

Kwon, Y.W., Bang, H., 2000. The Finite Element Method using MATLAB. CRC Press, New York.

Leung, A.Y.T., Su, R.K.L., 1995. Mixed-mode two-dimensional crack problem by fractal two level finite element method. Engineering Fracture Mechanics 51 (6), 889–895.

Marc, A.M, Krishan, K.C., 1999. Mechanical Behavior of Materials. Prentice-Hall, Inc., Upper Saddle River, NJ.

Menčík, J., 1992. Strength and Fracture of Glass and Ceramics. Elsevier Science Publishers, New York.

Mote Jr., C.D., 1971. Global–local finite element. International Journal for Numerical Methods in Engineering 3, 565–574.

Mukhopadhyay, N.K., Kakodkar, A., Maiti, S.K., 1998. Further considerations in modified crack closure integral based computation of stress intensity factor in BEM. Engineering Fracture Mechanics 59 (3), 269–279.

Mukhopadhyay, N.K., Maiti, S.K., Kakodkar, A., 2000. Variable singularity boundary element and its applications in computation of SIFs. Computers & Structures 77, 141–154.

Silvester, P., Cermark, I.A., 1969. Analysis of coaxial line discontinuities by boundary relaxation. IEEE Transaction on Microwave Theory and Techniques 17 (8), 489–495.

Sladek, J., Sladek, V., 1995. Boundary element analysis for an interface crack between dissimilar elastoplastic materials. Computational Mechanics 16, 396–405.

Su, B., Dunn, M.L., Lee, Y.C., 2001. Prediction of the crack initiation of GaAs in a soldered assembly. In: Proceedings of InterPACK'01, The PACIFIC RIM/International, Intersociety, Electronic Packaging Technical/Business Conference & Exhibition, July 8–13, 2001, Kauai, Hawaii, USA.

Tan, M., Meguid, S.A., 1996. Dynamic analysis of cracks perpendicular to bimaterial interfaces using a new singular finite element. Finite Elements in Analysis and Design 22, 69–83.

Thatcher, R.W., 1975. Singularities in the solution of Laplace's equation in two dimensions. Journal of the Institute of Mathematics and Its Applications 16, 303–319.

Thatcher, R.W., 1978. On the finite element method for unbounded region. SIAM Journal on Numerical Analysis 15, 466–477.

Xiao, F., Hui, C.Y., 1994. A boundary element method for calculating the K field for cracks along a bimaterial interface. Computational Mechanics 15, 58–78.

Wang, R.D., 1997. The stress intensity factors of a rectangular plate with collinear cracks under uniaxial tension. Engineering Fracture Mechanics 56 (3), 347–356.

Yan, A.M., Nguyen-Dang, H., 1995. Multiple-cracked fatigue crack growth by BEM. Computational Mechanics 16, 273–280.

Ying, L.A., 1978. The infinite similar element method for calculating stress intensity factors. Scientia Sinica 21 (1), 19–43.

Ying, L.A., Pan, H., 1981. Computation of K_I and compliance of arch shaped specimen by the infinite similar element method. Acta Mechania Solids Sinica 1, 99–106.

Ying, L.A., 1992. An introduction to the infinite element method. Mathematics in Practice Theory 2, 69–78.

Yoshida, K., Nishimura, N., Kobayashi, S., 2001. Application of new fast multipole boundary integral equation method to crack problems in 3D. Engineering Analysis with Boundary Elements 25, 239–247.

Yosibash, Z., Szabó, B., 1995. The solution of axisymmetric problems near singular points and computation of stress intensity factors. Finite Elements in Analysis and Design 19, 115–129.